Delayed Stormflow Generation in a Semi-humid Forested Watershed Controlled by Soil Water Storage and Groundwater Dynamics

Zhen Cui, Fuqiang Tian*

Department of Hydraulic Engineering, State Key Laboratory of Hydroscience and Engineering, Tsinghua University, Beijing 100084, China.

Corresponding author: Fuqiang Tian (tianfq@tsinghua.edu.cn)

Key Points:

- Threshold dynamics between soil water content and groundwater levels govern delayed stormflow generation.
- Groundwater fluctuations regulate the timing, magnitude, and merging of delayed and direct stormflow peaks.
- Hydrological connectivity and hydraulic conductivity increase with rising groundwater levels, driving delayed stormflow.

Abstract

Recent research by Cui et al. (2024) identified a distinct threshold governing bimodal rainfall-runoff events in a semi-humid mountainous forested watershed in North China, where delayed stormflow ~~appeared to be~~was influenced by shallow groundwater dynamics. Building on these findings, this study further investigates~~delves deeper into~~ the mechanisms driving these bimodal events, focusing on the interactions between soil water content (SWC) and groundwater level (GWL) during storm events. The results show that delayed stormflow is primarily governed by the interplay between SWC and GWL. Delayed stormflow is initiated when SWC exceeds the soil's water storage capacity, while its timing and magnitude are further modulated by GWL fluctuations. During rainfall, SWC increases rapidly but stabilizes after the rain ceases if the soil's water-holding capacity is not reached. Conversely, when SWC surpasses the storage capacity, the excess rainwater infiltrates into the subsurface, recharging groundwater and causing a gradual rise in GWL. As GWL rises, enhanced hydraulic conductivity facilitates the lateral movement of shallow groundwater toward the stream channel, generating delayed stormflow. ~~Concurrently, the effective connectivity between the stream channel and adjacent hillslopes increases in the vertical dimension.~~ When the GWL surpasses a critical threshold,~~At higher GWL thresholds,~~ its~~GWL~~ responses across the watershed become synchronized, significantly boosting groundwater discharge and reducing lag times. In extreme cases, the delayed stormflow peak converges with the direct stormflow peak. These findings enhance~~advance~~ the understanding of delayed stormflow mechanisms in semi-humid mountainous watersheds and refine~~, contributing to refining~~ runoff generation theories by elucidating~~providing insights into~~ the threshold-driven processes governing~~that govern~~ the timing and magnitude~~volume~~ of delayed stormflow.

Keywords: Delayed stormflow; Soil water storage; Groundwater outflow; Stormflow generation mechanism; Hydraulic conductivity

1. Introduction

Stormflow processes in the Xitaizi Experimental Watershed (XEW), located in North China, frequently exhibit~~exhibit a frequent occurrence of~~ bimodal stormflow hydrographs (Fig. A1), which often associated with~~lead to~~ significant stormflow and associated localized inundation. Analysis of 15 such events over the past decade revealed that the onset of these bimodal hydrographs is governed by threshold behavior. Specifically, delayed streamflow peaks tend to emerge when the combined total of event rainfall and antecedent soil moisture index exceeds 200 mm. The authors' findings suggest that shallow groundwater contributions are primarily responsible for these delayed stormflow events (Cui et al., 2024). However, the mechanisms behind the development of these bimodal hydrographs, which represent complex emergent hydrological behaviors, remain poorly understood. Understanding the formation of delayed stormflow is critical for advancing our comprehension of runoff generation processes and improving flood forecasting.

Bimodal hydrographs, characterized by dual streamflow peaks, typically occur during the wetting-up phases of catchments. Extensive research has identified several factors that influence dual streamflow peaks, including antecedent soil moisture, antecedent precipitation, groundwater levels, soil water storage, and rainfall amount (Haga et al., 2005; Graeff et al., 2009; Anderson and Burt, 1978; Padilla et al., 2015; Martínez-Carreras et al., 2016). Despite these advancements, the specific mechanisms that lead to threshold behavior and how these mechanisms produce the diverse shapes of stormflow hydrographs are still inadequately explained. For instance, Martínez-Carreras et al. (2016) found that a delayed peak only occurred when watershed storage reached a critical threshold of 113 mm in their specific study area. However, the precise reasons for this threshold and the underlying processes remain unclear.

The occurrence of bimodal hydrographs reflects a nonlinear runoff response, which offers valuable insights into the complex interactions between rainfall and runoff. The nonlinear pattern, characterized by both the timing and magnitude of the response, plays a crucial role in understanding stormflow processes. Recent decades have seen an increase in research on nonlinear and threshold

changes in rainfall-runoff responses, contributing to a deeper understanding of stormflow generation mechanisms. Nonlinear patterns, often characterized by rapid runoff responses that may lead to flooding, have been extensively documented in recent decades (Detty and McGuire, 2010; Farrick and Branfireun, 2014; Graham et al., 2010; Tromp-van Meerveld and McDonnell, 2006a; Penna et al., 2011; Scaife et al., 2020). However, many studies have yet to fully~~fail to~~ explore the intricate post-threshold mechanisms of these nonlinear shifts, leaving a gap in our understanding of stormflow generation across various catchments. While threshold behaviors are widely recognized, the detailed processes governing these shifts and their subsequent runoff dynamics remain underexplored.

Bimodal stormflow responses present an opportunity to investigate the relationship between rainfall thresholds and runoff generation, offering new perspectives on the timing and variability of stormflow. Despite this, many studies fail to distinguish between unimodal and bimodal streamflow responses. For example, Detty and McGuire (2010) focused on hydrological threshold responses but did not differentiate between unimodal and bimodal hydrographs, as their study primarily addressed general nonlinear rainfall-runoff processes~~ in general~~. Similarly, Martínez-Carreras et al. (2016) observed delayed peaks and identified catchment storage as a key factor influencing streamflow responses. H~~, h~~owever, they did not explicitly differentiate the underlying mechanisms between unimodal and bimodal responses. Such limitations often arise because the second peak in bimodal responses typically occurs after the rainfall event has ended, whereas many studies focus on streamflow changes during the event~~ itself~~. Additionally, bimodal responses are influenced by catchment-specific topography and geology, making them less observable in certain regions. These challenges highlight the need for a deeper~~more in depth~~ understanding of ~~investigation into~~ bimodal streamflow responses~~ to enhance our understanding of their mechanisms. Therefore, an in-depth investigation into the mechanisms driving these responses is essential~~. Such research would enable the grouping of similar hydrologic responses and facilitate comparisons of stormflow generation processes across different watersheds (Graham and McDonnell, 2010; Tromp-van Meerveld and McDonnell, 2006a, b).

Numerous~~Extensive~~ studies across diverse regions have explored the role of soil water content

and groundwater levels in generating delayed peaks in stormflow. Detty and McGuire (2010) emphasized subsurface flow thresholds in a forested catchment in the USA, while Farrick and Branfireun (2014) analyzed soil moisture and groundwater interactions in Canadian wetlands. Penna et al. (2011) examined antecedent soil moisture and storage thresholds in alpine catchments in New Zealand. These studies, along with others from ~~regions such as~~ Japan (Haga et al., 2005) and Europe (Graeff et al., 2009), contribute to our understanding of~~the growing body of knowledge on~~ threshold behavior in stormflow ~~responses~~. However, while these studies highlight the occurrence of thresholds, the complex interactions that drive post-threshold runoff processes remain insufficiently understood.

Investigating stormflow events in semi-humid regions, such as XEW, is challenging due to the relatively arid climate and low runoff coefficients. Over nearly a decade, 95 storm events were identified and analyzed in XEW, offering a rare and valuable dataset for examining bimodal stormflow responses in such regions. This study builds on prior findings to uncover the processes underlying delayed stormflow patterns. We hypothesize that the generation of delayed stormflow is governed by threshold-dependent interactions between soil water content (SWC) and groundwater level (GWL). The primary objectives of this study are: (1) to analyze the temporal dynamics of SWC and GWL during storm events, (2) to elucidate the mechanisms driving the threshold behavior observed in bimodal hydrographs, and (3) to reveal the underlying processes responsible for delayed stormflow in XEW.

2. Materials and methods

2.1 Study site

The study was conducted in the Xitaizi Experimental Watershed (XEW), a 4.22 km² catchment located in North China (40°32′N, 116°37′E), approximately 70 km northeast of Beijing ~~at~~ (Fig. 1). The watershed's elevation ranges from 676 m to 1201 m above sea level, and the region experiences a monsoon-influenced semi-humid climate. The average annual precipitation is 625 mm, with 80% concentrated between June and September. The mean annual temperature is 11.5°C with an average relative humidity of 59.1%. Forests cover 98% of the watershed, with broad-leaved species and

shrubberies accounting for 54.2% and 33.0%, respectively.

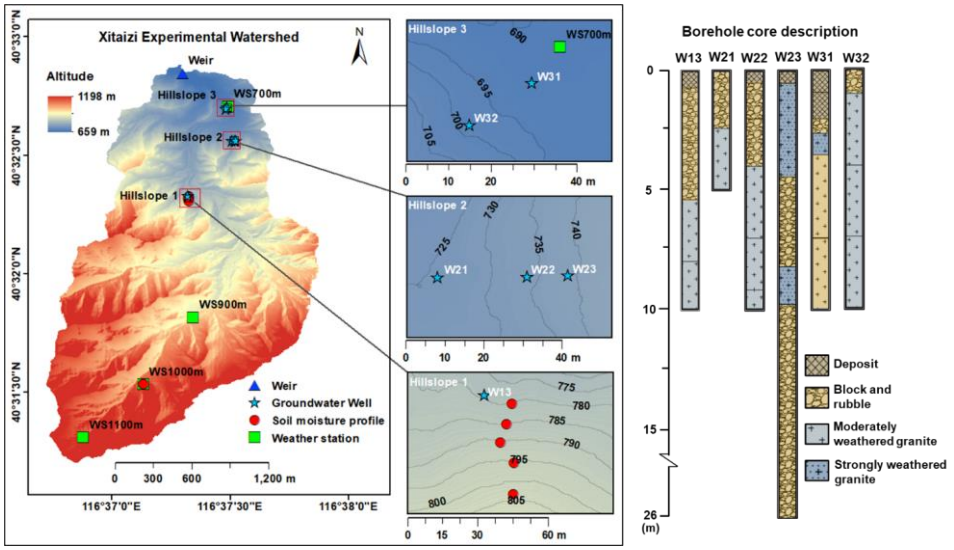

Figure 1. Location of Xitaizi Experimental Watershed (XEW) and a simple description of the borehole cores. This figure shows the distribution of monitoring instruments, including four weather stations (WS700, WS900, WS1000, and WS1100), an outlet weir, six groundwater observation wells, and eight soil moisture observation profiles. Of the eight soil moisture profiles, five are located on Hillslope 1, while the remaining three are positioned on the slope near WS1000. Research hillslopes (Hillslope 1, Hillslope 2, and Hillslope 3) are delineated as key zones for hydrological and geological investigations.

The soils in XEW are primarily brown earth and cinnamon soils, with a maximum depth~~s up to~~of 1.5 m and an average saturated hydraulic conductivity of 1.25×10^{-5} m/s~~45 mm/h~~. The surface soil is rich in organic matter, enhancing infiltration and reducing surface runoff potential. Underlying geology is predominantly compacted~~,~~ and deeply weathered granite, covering ~~(~~80% of the area~~)~~, with smaller portions of gneiss and dolomite. Fractured granite facilitates vertical and lateral subsurface flow, contributing to delayed groundwater responses. Slug tests estimated that the saturated hydraulic conductivity of weathered granite ~~to~~ ranges from 6.02×10^{-8} m/s~~5.2×10⁻³ m/day~~ to 1.34×10^{-5} m/s~~1.16 m/day~~.

2.2 Research hillslopes and instrumentation

Three research hillslopes (Hillslope 1, Hillslope 2, and Hillslope 3) were selected to investigate hydrological processes under varying geological and topographical conditions. Hillslope 1 (HS1) features thick soils overlying fractured granite, Hillslope 2 (HS2) has a highly permeable fractured block layer, and Hillslope 3 (HS3) consists of shallow soils over weakly weathered bedrock.

To capture spatial variability, SWC probes and boreholes were installed along hilltops, mid-slopes, and foot-slopes. Groundwater boreholes, ranging from 5 m to 26 m deep, were equipped with HOBO capacitance water level loggers to record GWL~~s~~ (Fig. 1).

2.3 Meteorological and streamflow data collection

Meteorological data spanning eleven years, from 2013 to 2023, ~~2013–2023~~ were collected from four GRWS100 automatic weather stations (WS700, WS900, WS1000, and WS1100), positioned at elevations of 700 m, 900 m, 1000 m, and 1100 m, respectively. Rainfall was recorded at 10-minute intervals using six tipping-bucket rain gauges near the weather stations, and the data were spatially averaged across the gauges for each time step for analysis.

Streamflow was measured at the catchment outlet using a Parshall flume, with water levels logged every 5 minutes since 2014. Data from some events were excluded due to sensor malfunctions or poor data quality, including key rainfall events in 2018 and 2019. Despite these exclusions, 95 rainfall-runoff events were analyzed, offering robust data for investigating bimodal stormflow characteristics.

2.4 Soil water content and groundwater level monitoring

Volumetric SWC was monitored at eight sites using CS616 time-domain reflectometry (TDR) probes installed at 10 cm intervals from the surface to 80 cm depth. Five profiles were located along HS1, and three were near WS1000. Measurements were recorded every 10 minutes, and the arithmetic mean of SWC values across the monitoring sites was computed for each time step.~~was used for~~

设置了格式: 字体: (中文) +中文正文 (宋体)

带格式的: 标题 2, 缩进: 首行缩进: 0 厘米

~~analysis.~~

GWLs (below the ground surface, hereinafter referred to as bgs) were observed in six boreholes distributed across the hillslopes. Hourly data were recorded using HOBO capacitance water level loggers~~ recorded hourly data~~. To facilitate comparisons across wells with varying absolute GWL ranges, we normalized the GWLs ~~were normalized using~~following the method described by Detty and McGuire (2010). ~~This normalization, expressed as the GWL index (I_G), standardizes GWLs across wells with varying ranges.~~

~~Groundwater levels were normalized following the method described by Detty and McGuire (2010).~~ Specifically, ~~For~~ for each well~~ and event~~, ~~the median height of the water table above the lowest recordable depth of the instrument was calculated and~~GWLs were normalized to ~~the~~ their total observed range, assigning a value of~~where~~ 0 to the shallowest GWL~~represents the minimum height~~ and 1 to the deepest~~represents the maximum height~~. The arithmetic means of these normalized values across all boreholes.~~This normalized value was~~ referred to as the groundwater index (I_G)~~.~~ , effectively~~We used I_G to facilitate comparisons across wells with different absolute GWL ranges and to~~ represent the overall GWL dynamics in the watershed. Given that lower I_G values indicate higher GWLs, and higher I_G values correspond to deeper GWLs, figures presenting I_G trends (e.g., Fig. 12 and Fig. A1) use an inverted vertical axis to align visually with hydrological intuition.

Rainfall, streamflow, and SWC data were aggregated to hourly intervals for alignment with GWL data. Preliminary analysis confirmed that the delayed second streamflow peak had response times exceeding the hourly scale, rendering this aggregation sufficient for the study's purposes.

2.5 Rainfall-runoff event identification and hydrograph analysis

Rainfall events were identified using an intensity-based automatic algorithm~~ described by~~ (Tian et al.~~ (~~, 2012) that defines an event as periods with hourly-averaged rainfall intensity exceeding ~~≥~~0.1 mm/h, separated by at least six consecutive hours with intensities below this threshold~~and a minimum separation of six hours between events~~. Events with cumulative rainfall

~~exceeding~~ > 5 mm were retained for analysis~~analyzed~~.

Bimodal rainfall-runoff events were manually identified based on two criteria: (1) the presence of a secondary, arch-shaped runoff peak occurring after rainfall cessation or during minimal intermittent rainfall, and (2) ~~A~~ a distinct separation between the direct (sharp) and delayed (broad) peaks. Further~~More~~ details ~~of~~ on~~the~~ classification can be found~~are described~~ in Cui et al. (2024~~,~~ ~~HESS~~).

The combination of automatic event delineation and manual identification ensured the accurate selection of 14 rainfall-runoff events with well-defined delayed peaks for subsequent analysis. Streamflow was separated into storm runoff and baseflow using the HYSEP program with the constant slope method (Hewlett and Hibbert, 1967; Sloto ~~&~~ and Crouse, 1996), supplemented by manual adjustments for complex hydrographs. ~~Event stormflow volumes were calculated as total discharge minus baseflow.~~

~~Streamflow was separated into storm runoff and baseflow using the HYSEP computer program with the constant slope method, supplemented by manual adjustments for complex hydrographs.~~ Throughout the manuscript, stormflow refers to the total discharge, while~~and~~ event stormflow volume~~s~~ (q_s) ~~were~~ is calculated as the total discharge minus baseflow~~, which are expressed in q_s~~.

2.6 Hydrological connectivity analysis

Hydrological connectivity among streamflow, SWC, and GWL ~~was~~ were analyzed to examine the interplay of subsurface flow pathways. Rainfall-runoff events were analyzed based on their total rainfall (> 5 mm) and corresponding streamflow peaks. As illustrated in Fig. 2, ~~The~~ the peak rainfall intensity (R_p) was determined based on the maximum 1 ~~hour~~h rainfall intensity, with the time of occurrence recorded as TP_p. Metrics such as initial streamflow (Q_0) and peak streamflow (Q_p) were determined alongside their respective ~~timings~~ times (TQ_0 and TQ_p).

Similar metrics were calculated for SWC and GWL, including initial values (SWC_0 and I_{G0}) and peak values (SWC_p and I_{Gp}), with corresponding times of occurrence (TS_0, TI_{G0}, TS_p, and TI_{Gp}). These

设置了格式: 非上标/ 下标

metrics allowed for a comprehensive evaluation of the soil water-groundwater-streamflow response relationship across 95 distinct rainfall-runoff events.

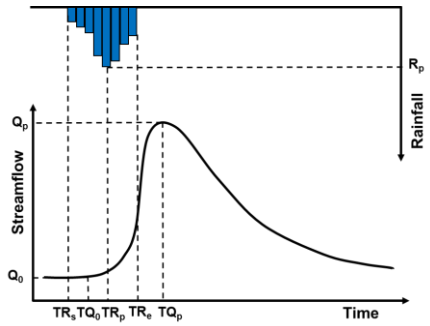

Figure 2. Conceptual framework of rainfall event analysis.

3. Results

3.1 Hillslope-scale dynamics of SWC and GWL during rainfall-runoff events

The temporal evolution of SWC and GWL was analyzed across 95 rainfall-runoff events to understand their dynamic interaction. Our analysis revealed a clear relationship between SWC and GWL dynamics, with SWC initially increasing rapidly during rainfall, followed by ~~a~~ stabilization or a decline once a threshold was reached. In contrast, GWL showed a more delayed response (Fig. 3). Three distinct patterns of SWC and GWL interaction were identified.

Figure 3 illustrates the dynamics of SWC and GWL during three representative events. These events were selected to demonstrate the variability in SWC and GWL patterns identified across the 95 rainfall-runoff events. The selected events all occurred within the same year to minimize inter-annual variability and ensure comparability. Red circles indicate rainfall periods, while black circles represent post-rainfall periods. Under dry conditions, despite receiving 66.6 mm of rainfall, SWC remained relatively low (< 0.20 m^3/m^3), exhibiting a gradual increase during the rainfall event and stabilizing thereafter. In contrast, GWL displayed minimal response (Fig. 3a).

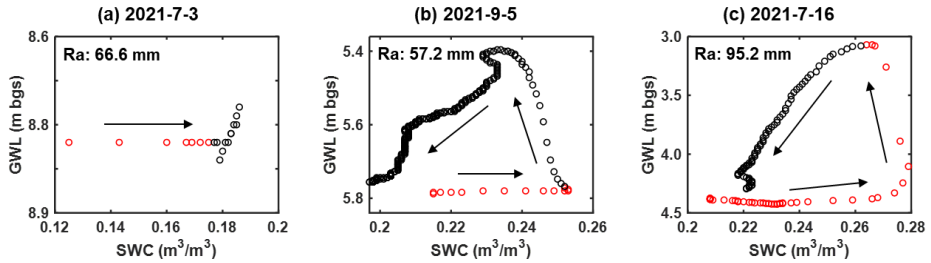

Figure 3. Three typical SWC-GWL dynamics patterns during rainfall-runoff events. Ra represents~~is~~ rainfall amount. Arrows indicate the temporal evolution of the events. Red circles indicate periods of rainfall, whereas~~while~~ black circles denote post-rainfall periods.

In events with wet conditions, both SWC and GWL showed significant increases. However, the timing of GWL rise varied: in some cases, GWL rose after the cessation of rainfall, while in other cases, it began rising before the rainfall ended. The primary distinction between these patterns lies in the timing of the GWL rise: in Fig. 3b (57.2 mm rainfall), GWL began to rise after the rainfall ceased~~ended~~, whereas in Fig. 3c (95.2 mm rainfall), GWL started to rise noticeably before ~~the end of the~~ rainfall ended.

In the case represented by Fig. 3b, SWC increased significantly, surpassing 0.20 m^3/m^3, while GWL showed a delayed rise after the rainfall ceased. ~~The~~ A counterclockwise hysteresis was observed as SWC continued to increase while GWL remained largely unchanged during rainfall. Fig. 3c, which typically represents intense storm events, showed a sharp increase in both SWC and GWL, with SWC exceeding 0.25 m^3/m^3. GWL began to rise before the rainfall ended, reaching a peak as rainfall continued, and both variables showed a substantial decline after rainfall ceased. These representative events highlight the variability in the SWC-GWL relationship, including~~with~~ timing differences in the rise of GWL and distinct hysteresis patterns during moderate and extreme events.

We further quantified the frequency distribution of SWC and GWL increases or decreases across the 95 rainfall-runoff events (Fig. 4). Notably, in 49 events, SWC increased, while GWL increased in 43 events. In contrast, SWC declined in 26 events and GWL declined in 15 events. Notably~~Importantly~~, 15 events showed a simultaneous decline in both SWC and GWL, which ~~were~~

was associated with delayed stormflow and larger stormflow volumes. One such event, on August 15, 2021, exhibited fluctuating SWC and GWL values throughout the rainfall event due to the more dispersed rainfall distribution. As a result, our subsequent analysis primarily focused on the remaining 14 events with well-defined response characteristics.

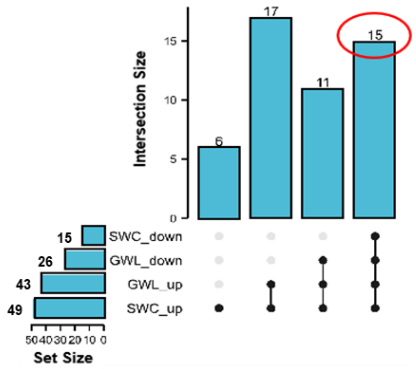

Figure 4. UpSet plot of the response characteristics of SWC and GWL during rainfall-runoff events.

3.2 SWC dynamics across rainfall-runoff events

Figure 5 presents the SWC dynamics observed during 14 distinct rainfall-runoff events, each characterized by minimal or no intermittent rainfall during the recession period. To facilitate a clear comparison of SWC changes across events, the peak of each event was aligned with a horizontal axis value of 0.

During the initial rainfall phase, SWC increased rapidly, reaching a peak value. As the rainfall ceased, SWC began to decline, though at a slower rate, eventually stabilizing at a specific value. To quantify the threshold at which SWC stabilizes, we conducted a statistical analysis of the stabilized~~stable~~ SWC during these events. The stable phase was defined as the period following the recession phase when SWC exhibited minimal variation before subsequent rainfall. The statistical analysis of the stable SWC revealed a mean ~~value~~ of 0.197~~4~~ ± 0.004 m^3/m^3, with ~~a standard deviation of 0.0158 and~~ a 95% confidence interval of 0.188 – 0.207~~[0.1945, 0.2003]~~ m^3/m^3. These results

validate the visually observed threshold of 0.20 m³/m³ for SWC stabilization. The general pattern of SWC variation is schematically illustrated in Fig. 6.

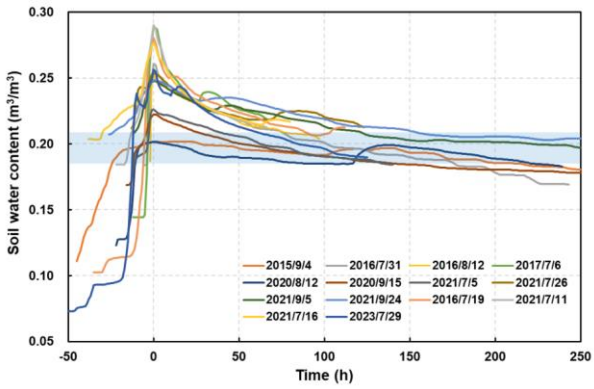

Figure 5. SWC dynamics during different storm events. The blue strip indicates the 95% confidence interval of stable SWC.

The SWC response to rainfall is rapid. Upon rainfall onset, SWC increased sharply. Once the rainfall ceased, the subsequent behavior of SWC ~~depends~~ depended on whether the peak value ~~exceeds~~ exceeded the 0.20 m³/m³ threshold. If SWC remains below or at 0.20 m³/m³, it either stabilizes or declines slowly. However, when SWC exceeds 0.20 m³/m³, it decrease~~d~~ rapidly before stabilizing around the 0.20 m³/m³ threshold. The magnitude of the peak above 0.20 m³/m³ influences the speed of the subsequent decline in SWC: the greater the peak, the faster the decline.

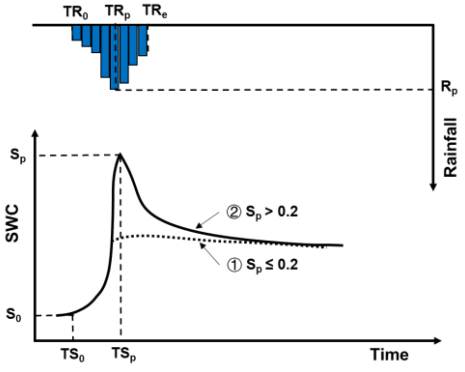

Figure 6. Conceptual diagram of SWC response during storm events. S_p is the maximum SWC value.

3.3 GWL dynamics and response types

This section examines GWL dynamics during 14 selected rainfall-runoff events, chosen for their clear and consistent GWL and SWC patterns. These events facilitate a detailed investigation into groundwater response to storm events. Two distinct GWL response types—quick and slow—were identified and are conceptually illustrated in Fig. 7. It is important to note that Fig. 7 is a conceptual representation, not based on specific rainfall-runoff events, and does not include rainfall depth data.

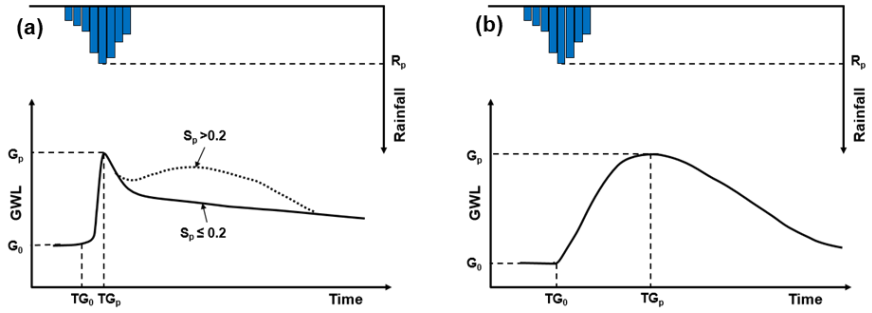

Figure 7. Conceptual diagram of GWL response during storm events. G_0 and G_p represent the initial and maximum values of GWL, respectively. S_p denotes the maximum SWC value.

In events exhibiting a quick response, the GWL rises rapidly, closely aligning with the SWC peak. The GWL response typically lags behind the SWC peak, ranging from ~~by~~ 0 h to 6 h (Fig. 7a). For events where SWC exceeds 0.20 m^3/m^3 (and particularly when it surpasses 0.24), the GWL often shows a secondary rise following the initial peak, as indicated by the dotted line in Fig. 7a. Conversely, the slow response occurs when SWC declines sharply after reaching its peak, resulting in a delayed rise in GWL (Fig. 7b).

An analysis of GWL responses across various hillslopes revealed spatial variability. For instance, the GWL at HS2 (wells W21~~–~~23) exhibited a quick response (Fig. 7a), whereas the GWL~~s~~ at HS1 (W13) and HS3 (W31 and W32) displayed slow response characteristics (Fig. 7b). These findings

suggest that the GWL dynamics are influenced not only by SWC but also by the underlying geological structure of each hillslope.

At the watershed scale, GWL response to storm events demonstrated considerable spatial variability. I_G, which represents the average normalized GWL across multiple wells, was used to capture catchment-scale groundwater response~~an integrated view~~. ~~Analysis revealed that~~ I_G often exhibited two distinct peaks during storm events. Among the 14 events analyzed, 9 events displayed dual I_G peaks, coinciding with the two peaks in streamflow. However, at the individual well level, only W13 (HS1) and W23 (HS2) exhibited dual GWL peaks. Specifically, W13 showed two peaks during one event, while W23 exhibited two peaks during five events. The remaining wells displayed only a single peak across all events analyzed (see Table 1).

Table 1. Statistical results of response characterization of streamflow, I_G and groundwater levels.

			HS1	HS2			HS3	
	Streamflow	I_G	**W13**	**W21**	**W22**	**W23**	**W31**	**W32**
Total number of events	14	14	14	8	14	14	9	9
Number of events with two peaks	9	9	1	0	0	5	0	0

3.4 GWL responses across hillslope positions

Further examination of GWL responses across various locations is presented in Fig. 8, which shows the magnitude of GWL increases and their lag times relative to rainfall onset. While variations in GWL were observed among the monitoring wells, the differences in GWL increments were generally modest, with mean increases ranging from 1 m to 2 m. Notably, smaller GWL changes were recorded at the foot of the hillslope (e.g., W21 and W31). Within the same hillslope, GWL increments tended to increase progressively from the foot to the top, as seen in HS2 (W21~~-~~W23) and HS3 (W31 and W32).

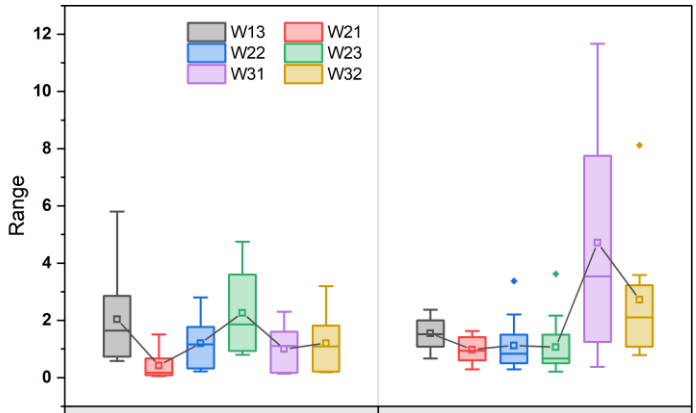

	△GWL (m)						Lag time (day)					
Location	W13	W21	W22	W23	W31	W32	W13	W21	W22	W23	W31	W32
Min	0.6	0.1	0.2	0.8	0.1	0.2	0.7	0.3		0.2	0.4	0.8
Max	5.8	1.5	2.8	4.8	2.3	3.2	2.4	1.6	3.4	3.6	11.7	8.1
Mean	2.0	0.4	1.2	2.3	1.0	1.2	1.5	1.0	1.1		4.7	2.7

Figure 8. GWL increments (ΔGWL) and lag time of peak GWL relative to rainfall onset at different locations.

In contrast, the lag times for maximum GWL exhibited greater variation across locations. For instance, at HS3, lag times ranged from 0.4 d to 11.7 d at W31 and from 0.8 d to 8.1 d at W32, significantly longer than those at HS1 (0.7–2.4 d) and HS2 (0.2–3.6 d). Interestingly, within a single hillslope, no consistent relationship was found between the lag time of maximum GWL and its distance from the foot of the hillslope.

To further investigate these dynamics, the relationship between GWL increments and SWC was analyzed across 14 storm events (Fig. 9). The analysis focused on six observation wells (W13, W21–W23, W31, and W32) located on three hillslopes (see Fig. 1 for well locations). The variability in GWL response types—quick versus slow—~~was~~ were attributed to spatial differences in SWC thresholds and hillslope geological structures.

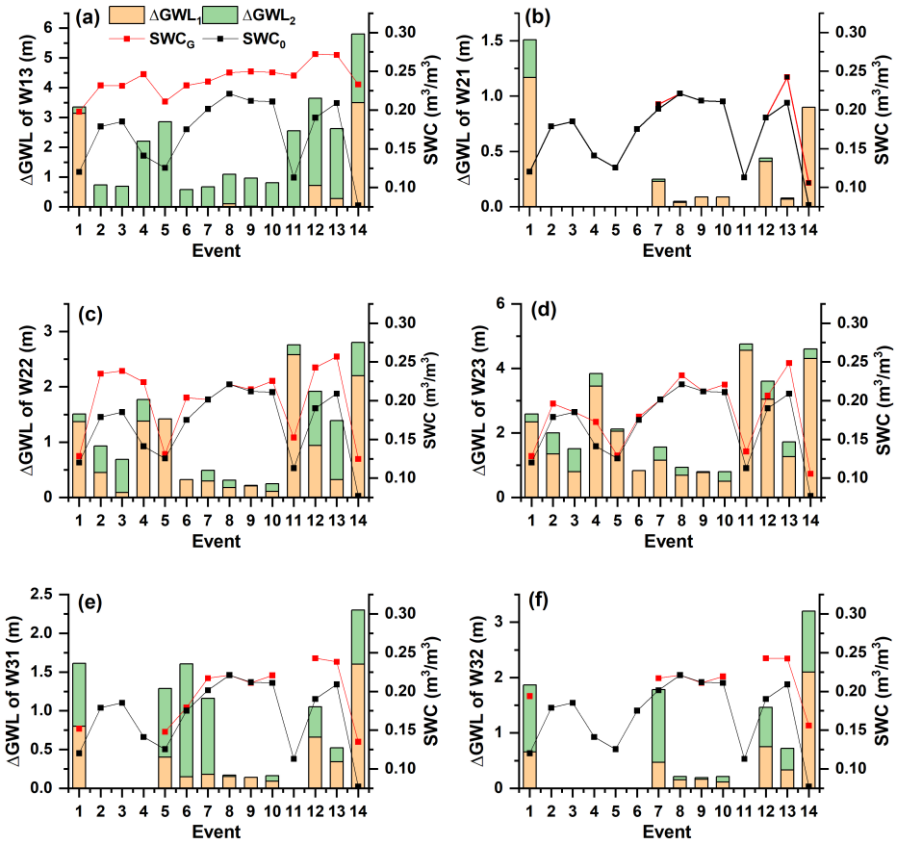

Figure 9. GWL increments (ΔGWL) across various locations during 14 storm events, along with initial SWC (SWC_0) and SWC at the onset of GWL rise (SWC_G). The orange bars represent ΔGWL during the SWC increase phase, while the green bars represent ΔGWL during the SWC decline phase. The red and black lines denote SWC_G and SWC_0, respectively.

In Fig. 9, the orange bars represent GWL increments during the SWC increase phase (up to its peak), while the green bars indicate GWL increments during the SWC decline phase (from its peak to when GWL reached its maximum). The black and red dotted lines mark the initial SWC (SWC_0) and the SWC at the onset of GWL rise (SWC_G), respectively. Missing data for some locations are indicated by the absence of bars in Figs. 9b, 9e, and 9f.

The analysis revealed that the magnitude of the SWC increase following rainfall onset is a key determinant of delayed GWL responses. Specifically, a greater difference between SWC_G and SWC_0 corresponded to ~~an~~ the onset of GWL rise ~~begins~~. Conversely, when SWC_G and SWC_0 ~~are~~ were similar, GWL rose almost simultaneously with the SWC increase.

At HS1 (W13), GWL began to rise only after SWC exceeded 0.20 m^3/m^3. Most of the GWL increase occurred during the SWC decline phase, suggesting that soil wetness exerts a threshold effect on GWL dynamics. This delayed response aligns with the slow response type. At HS2 (W21~~–~~23), GWL responses were more immediate, with GWL increases closely following SWC rises. SWC_G values at these locations ranged widely (from 0.13 m^3/m^3~~-~~ to 0.26 m^3/m^3) but were generally close to SWC_0, indicating that GWL responses at HS2 are less dependent on SWC thresholds and exhibit a quick response type.

HS3 demonstrated both quick and slow GWL responses. Initial rises occurred soon after the onset of the SWC increase, but the majority of GWL increments took place during the prolonged SWC decline phase following its peak. This pattern suggests a more complex interaction of immediate and delayed factors influencing GWL dynamics at HS3.

These findings highlight a strong relationship between the emergence of quick and slow GWL response types and SWC dynamics. In quick response types, GWL increments occur primarily during the SWC increase phase, resulting in a steep response curve. In slow responses, GWL increments predominantly occur during the SWC decline phase, producing an arch-shaped response curve. These distinctions underscore the pivotal role of SWC dynamics in regulating the timing and magnitude of GWL responses across different hillslopes.

3.5 Characterization of groundwater response at the watershed scale

Figure 10 illustrates the timing of I_G peaks relative to SWC response. The first I_G peak occurred rapidly following rainfall, initiating less than 2 h~~0–2 h~~ after the SWC began to rise and reaching its peak ~~occurring~~ 0 h ~~–~~to 9 h later (mean: 3.7 h) after SWC reached its maximum. In contrast, the second

I_G peak typically occurred post-rainfall, lagging behind the SWC peak by 10–65 h (mean: 28 h). These patterns align with the quick and slow GWL response types identified in ~~section~~ Section 3.2. The occurrence of dual I_G peaks can be attributed to the superimposition of groundwater contributions from different hillslopes with differing response rates. The first (quick) GWL response is tightly coupled to rainfall onset and SWC increases, while the second (slow) GWL response reflects gradual infiltration and groundwater recharge occurring over a broader timescale.

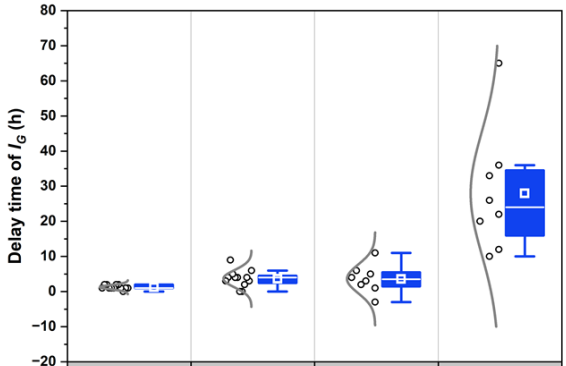

	Δt_1=TI_{G01}-TS_0	$\Delta t2$=TI_{Gp1}-TS_p	Δt_2=TI_{G02}-TR_e	Δt_4=TI_{Gp2}-TS_p
Min	0	0	−3	10
Max	2	9	11	65
Mean	1.3	3.7	3.6	28.0

Figure 10. Delay time of I_G peaks relative to peak SWC. TI_{G01} and TI_{G02} represent the onset times of the first and second peaks of I_G, respectively. TS_0 and TS_p indicate the time when SWC started to increase and peaked, respectively. TI_{Gp1} and TI_{Gp2} represent the time when I_G started to increase and peaked, respectively. TR_e indicates the end of rainfall.

The growth rates of I_G towards the two peaks were also quantified (Fig. 11). A notable disparity was observed between the growth rates of the first (r_1) and second (r_2) I_G peaks. The first I_G peak exhibited a markedly faster rate~~s~~ (ranging from 0.03 d^{-1} to 0.98 d^{-1}, with a mean of 0.38 d^{-1}~~0.03 to 0.98/day, mean: 0.38/day~~) ~~compared to~~than the second peak (ranging from 0.01 d^{-1} to 0.31 d^{-1}, with a mean of 0.07 d^{-1}~~0.01 to 0.31/day, mean: 0.07/day~~). These differences reflect the contrasting dynamics of quick and slow GWL responses across hillslopes. In events featuring dual I_G peaks, the maximum I_G was typically observed at the second peak. However, in events with higher GWLs

(indicating lower I_G), the disparity between the growth rates diminished, making the two peaks harder to distinguish (e.g., Events 9 and 10). In Events 11–14, where GWLs were significantly higher, only a single I_G peak was observed.

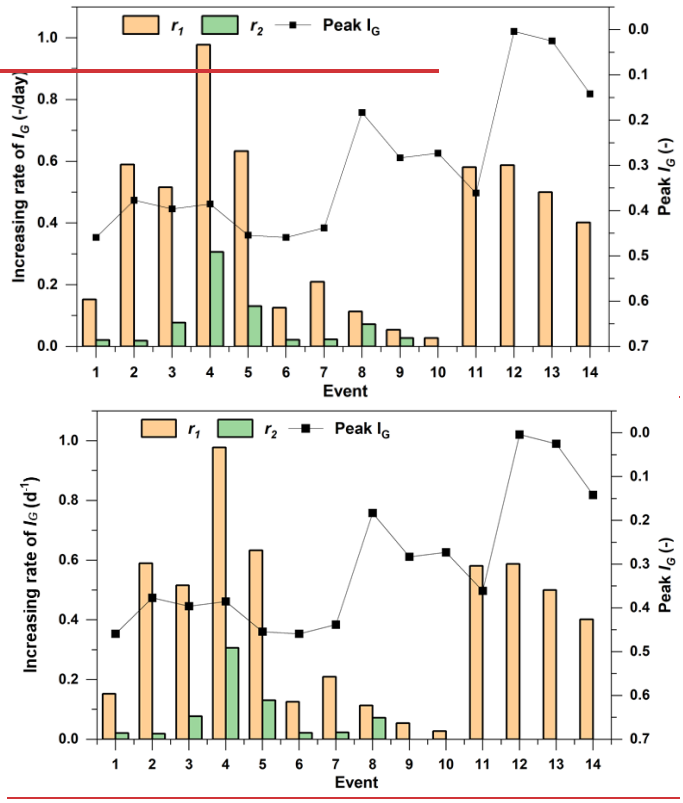

Figure 11. Growth rates of I_G and the maximum I_G value across storm events. r_1 and r_2 denote the ascent rates during the first and second peaks, respectively.

The contrasting dynamics of the two I_G peaks highlight their distinct formation mechanisms. The first I_G peak, occurring during rainfall, is closely associated with the rapid rise in SWC. Conversely, the second I_G peak emerges post-rainfall, coinciding with soil drainage~~draining~~ and groundwater recharge processes. As reported by Dang et al. (2023), rainfall induces pressure waves that rapidly expel soil water from the lower soil column, while infiltrated rainwater migrates

downwards at slower pace. ~~pressure~~Pressure-driven displacement generates a near-instantaneous GWL response during the initial phase of rainfall.

We conjecture that the rapid I_G peak is linked to kinematic wave triggered by increased SWC, which displaces pre-existing "old" soil water and groundwater, leading to a synchronized GWL rise (e.g., Anderson and Burt, 1978). Despite the slow percolation of water through soil and bedrock, the theoretical celerity of this kinematic response is near-instantaneous, accounting for the rapid GWL rise. Furthermore, drilling data suggest ~~that~~ the presence of faults in the bedrock of HS2, which may facilitate a~~potentially facilitating~~ faster groundwater response on this hillslope compared to others.

The second, slow I_G peak is likely driven by the gradual infiltration of rainwater into deeper soil and bedrock layers, ultimately recharging the groundwater. This process is regulated by the soil's water storage threshold. Before reaching this threshold, the soil retains all incoming rainfall. Once exceeded, excess water drains rapidly into deeper layers, leading to a decline in SWC and a concurrent rise in GWL due to groundwater recharge.

4. Discussion

4.1 Inter-hillslope GWL dynamics

GWL variations in lag times and response magnitudes across hillslopes can be attributed to differences in geological conditions. HS1 and HS3 are primarily underlain by fully to strongly weathered granite, with upper layers comprising significant soil-rock mixtures. These features lead to relatively slower GWL responses, likely due to the limited permeability of the regolith and underlying materials. In contrast, HS2 is characterized by a fractured rock layer at depths varying from 10 m to 30 m~~of 10-30 meters~~ (see Fig. 1), which enhances subsurface flow and facilitates faster GWL responses. These geological contrasts explain the observed differences in GWL response times among the hillslopes.

Among the three hillslopes, HS3 exhibited the slowest GWL responses, characterized by the longest lag times. This distinct behavior makes HS3 a crucial reference for understanding inter-

hillslope variations in GWL dynamics. A ~~Previous~~ previous study by Cui et al. (2024) highlighted that GWL response times are closely linked to delayed stormflow timing, emphasizing the importance of examining GWL dynamics. Comparing the GWL response times of HS1 and HS2 with those of HS3 provides insights into how geological structures and SWC thresholds influence delayed stormflow generation.

Furthermore, the deeply weathered regolith and extensive fracturing in HS2 promote more rapid stormflow generation, as water stored in the regolith layer contributes to streamflow over extended periods. This finding aligns with previous studies (Kosugi et al., 2011; Padilla et al., 2015), which demonstrated that geological features such as fracture density and weathering depth influence subsurface flow paths and, ultimately, groundwater dynamics.

To deepen understanding of the inter-hillslope differences in GWL responses, we calculated the lag times between rainfall onset and peak GWL responses for all observation wells on each hillslope, incorporating spatial variability. Average lag times, denoted as t_{S1}, t_{S2} and t_{S3} for HS1, HS2, and HS3, respectively, were used to calculate the time differences $\Delta t = t_{S1} - t_{S3}$ and $\Delta t = t_{S2} - t_{S3}$. These time differences were then analyzed for their correlation with I_G, as illustrated in Fig. 12.

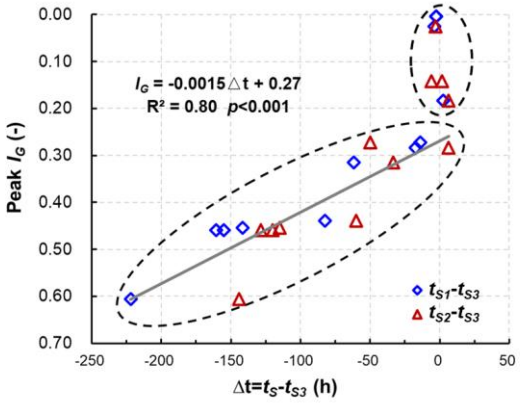

Figure 12. Correlation between peak I_G and the time differences from peak GWL responses on HS1, and HS2 to HS3 ($\Delta t = t_S - t_{S3}$), where t_{S1}, t_{S2} and t_{S3} are the average lag times of peak GWLs on HS1, HS2 and HS3, respectively. Note that the I_G axis is inverted: I_G is a normalized groundwater index where lower values indicate higher GWLs, and higher values represent deeper GWLs.

In Fig. 12, blue diamonds represent $\Delta t = t_{S1} - t_{S3}$, while red triangles represent $\Delta t = t_{S2} - t_{S3}$. Both pairs exhibit a significant negative correlation with peak I_G, as described by the equation: $I_G = -0.0015 \times \Delta t + 0.27$ ($R^2 = 0.80$, $p < 0.001$). These results indicate that lower I_G values correspond to shorter inter-hillslope lag times, suggesting enhanced hydrological connectivity and transmissivity feedback mechanisms, as described in previous studies (Kendall et al., 1999; Bishop et al., 2011).

As peak I_G approaches 0.30, Δt converges to near-zero with minimal fluctuations, particularly during extreme storm events. This finding supports the results presented in Fig. 11, which demonstrate that elevated GWLs synchronize GWL responses across the watershed. This synchronization reflects a critical hydrological mechanism driven by transmissivity feedback, which amplifies groundwater movement, reduces lag times, and enhances watershed-scale connectivity. This dynamic is consistent with the work of Padilla et al. (2015), who reported ~~that~~ shorter lag times in bedrock aquifers with high-transmissivity conduits, and with Scaife et al. (2020), who noted that increased connectivity during high GWL conditions reduces lag times and enhances watershed-scale hydrological responses.

Furthermore, although Fig. 12 uses ~~labels the vertical axis as~~ I_G to represent watershed-wide GWL status, a similar pattern emerges when substituting~~replacing~~ I_G with ~~site~~ site-specific GWL values, acknowledging that~~though the~~ GWL thresholds may vary among observation sites. These observations reinforce the idea that watershed-scale groundwater dynamics are influenced by the interplay between spatially variable geological conditions and temporal variations in GWL.

4.2 Delayed stormflow processes linked to GWL dynamics

Previous studies have shown that streamflow in XEW frequently exhibits a bimodal hydrograph during heavy rainfall, with delayed stormflow likely originating from shallow groundwater outflow (Cui et al., 2024). Understanding the timing and lag between groundwater and streamflow responses

is crucial for identifying dominant runoff generation mechanisms (Beiter et al., 2020). Discrepancies in these timings can indicate contributions from different water sources to the stream channel. Fig. 13 illustrates the relative timing of maximum I_G (I_{Gp}) and maximum SWC (SWC_p) for eight storm events, alongside rainfall duration.

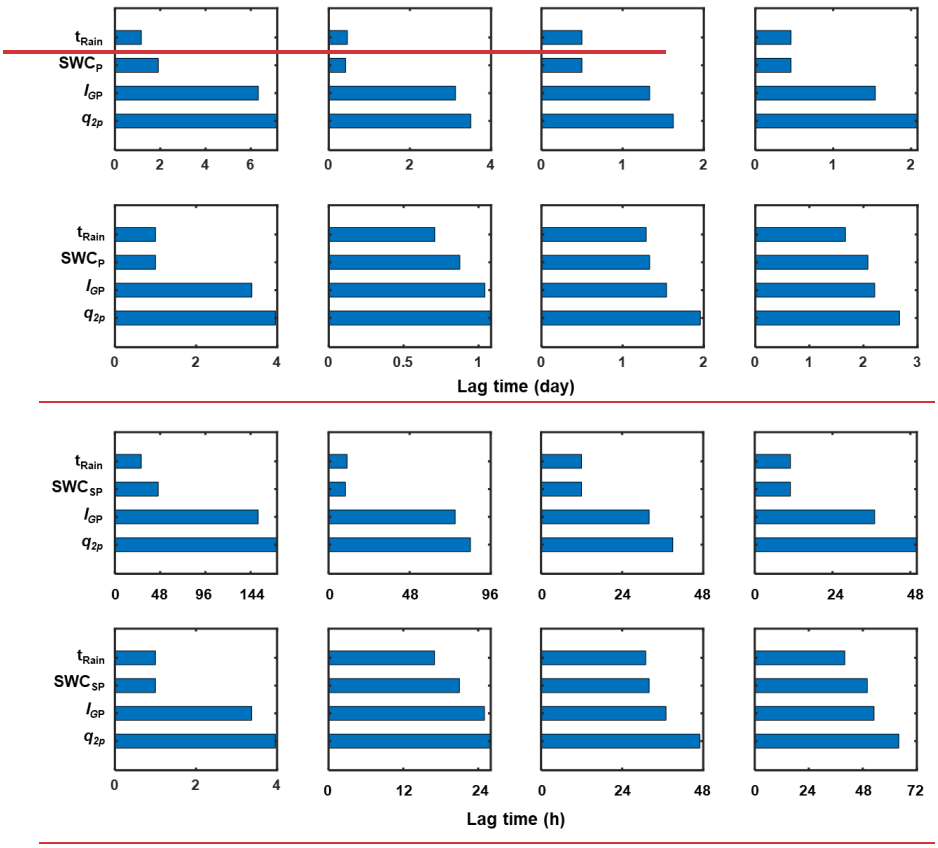

Figure 13. Lag times of maximum SWC and GWL relative to rainfall onset. Each bar indicates the rise and peak times of the corresponding variable, with t_{Rain} indicating rainfall duration. SWC_{SP} and I_{GP} represent the maximum SWC and I_G, respectively, while q_{2p} denotes the delayed streamflow peak.

Rainfall durations for the analyzed events ranged from ~~0.46~~11 h to ~~1.67~~40 ~~days~~h. SWC, I_G,

and delayed stormflow (q_{2p}) followed a clear sequence in their peak timings relative to rainfall onset. SWC responded rapidly, with its peak occurring ~~0.4~~10 h to ~~2.1~~50 ~~days~~ h after rainfall began, usually coinciding with or slightly after rainfall cessation. In contrast, I_G continued to increase after the SWC peak and reached its maximum before the delayed stormflow peak (q_{2p}). While the lag times between SWC_p, I_{Gp}, and q_{2p} varied among events, the lag between I_{Gp} and q_{2p} remained relatively consistent.

This pattern aligns with findings from Haught and Meerveld (2011) and Rinderer et al. (2016), who suggest that when groundwater response precedes or synchronizes with streamflow, it indicates strong hillslope-stream connectivity, with groundwater serving as the primary driver of streamflow. Our results corroborate this view, showing that q_{2p} timing is predominantly governed by groundwater dynamics. This relationship is further validated by the strong linear correlation between the lag times of q_{2p} (t_{2p}) and I_{Gp} (t_{IGp}), as indicated by the regression equation $t_{2p} = 1.11\times t_{IGp} + 0.17$, with a slope of 1.11, showing a high determination coefficient ($R^2 = 0.995$, $p < 0.01$). (Fig. 14).

Conversely, the correlation between t_{2p} and the lag time of SWC_p (t_{SWCp}) was weak ($R^2 = 0.029$, $p = 0.688$), indicating that the timing of SWC_p has minimal influence on the delayed streamflow peak. Additionally, the I_G pattern during the delayed stormflow period closely mirrored the shape of the streamflow hydrograph (Fig. A1), reinforcing the dominant role of I_G ~~plays~~ in controlling delayed stormflow.

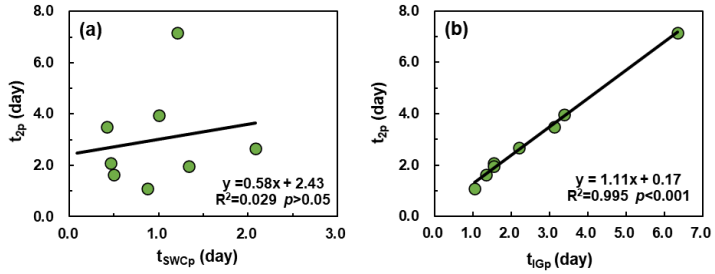

Figure 14. Lag times of maximum (a) SWC and (b) I_G relative to delayed streamflow peaks (t_{2p}). t_{SWCp} and t_{IGp} denote the peak times of the SWC and I_G, respectively.

~~Further q~~Quantitative analysis revealed a strong exponential relationship between streamflow

and I_G during the delayed stormflow period (Fig. 15). In the non-rainfall phase of the eight bimodal events, streamflow increased exponentially with GWL (IG_p), exhibiting a highly significant correlation ($p < 0.001$) and a determination coefficient of $R^2 = 0.90$. This exponential increase in streamflow is attributed to the increase in lateral hydraulic conductivity as the water table approaches the surface. Similar findings have been reported by Detty and McGuire (2010) and Kendall et al. (1999), where groundwater outflow dominates during storm events.

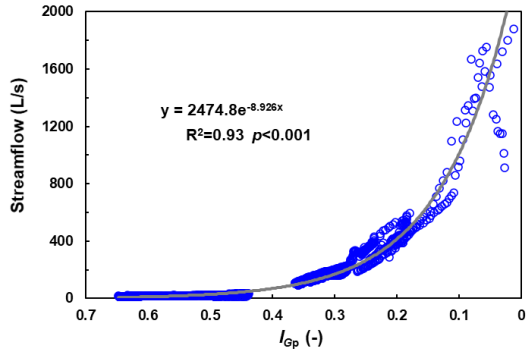

Figure 15. Correlation between I_G and streamflow during delayed stormflow periods.

At higher GWLs, the curve of GWL vs. streamflow begins to flatten, suggesting a feedback mechanism. As the rising water table mobilizes shallow groundwater outflow, water is rapidly transported to the stream via shallow flow paths. This process, often referred to as transmissivity feedback, is consistent with Lundin's (1982) description of groundwater dynamics during delayed stormflow periods.

4.3 Delayed stormflow processes linked to GWL dynamics

Understanding the critical thresholds that govern the movement of water within landscapes is essential for accurately predicting delayed stormflow, as emphasized by McDonnell et al. (2021). This study identified a strong ~~Relationship~~ relationship between delayed stormflow and the gradual response of GWL, primarily influenced by a sharp decline in SWC when it exceeds a critical threshold of 0.20 m^3/m^3.

To identify the threshold for delayed stormflow initiation in XEW, we analyzed 63 out of 95 rainfall-runoff events with complete streamflow data. The relationship between SWCp and q_s for these events is illustrated in Fig. 16. A clear threshold behavior emerged: when SWC remained~~was~~ below 0.20 m^3/m^3, q_s remained minimal, consistent with unimodal events. However, as SWC exceeded 0.20 m^3/m^3, ~~a noticeable increase in~~ q_s exhibited a noticeable increase~~was observed~~, indicating~~signaling~~ the initiation~~onset~~ of delayed stormflow in certain~~some~~ events. Specifically, when SWC surpassed 0.23 m^3/m^3, a pronounced surge in stormflow volume occurred, accompanied by the emergence of a secondary stormflow peak in all events. These findings suggest that the critical threshold for delayed stormflow initiation lies within the SWC range of 0.20 m^3/m^3 to 0.23 m^3/m^3.

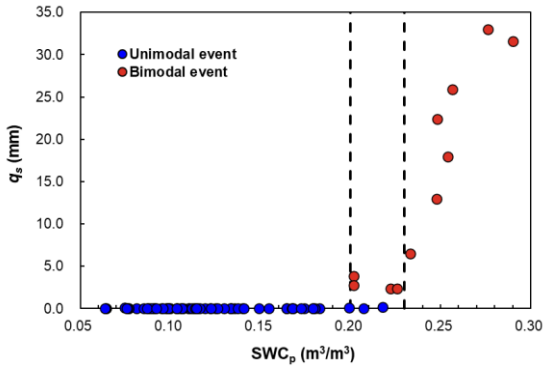

Figure 16. Relationship between maximum SWC (SWC_p) and event stormflow volume (q_s).

These results underscore the pivotal role of the surface soil layer's water deficit or water-holding capacity in triggering delayed stormflow. During rainfall events, the soil retains water until its water-holding capacity is exceeded. Once SWC surpasses the threshold of 0.20 m^3/m^3, the soil begins to release water more rapidly, initiating delayed stormflow. Additionally, during unimodal events, stormflow (q_s) remained consistently below 1 mm despite variations in SWC, indicating that stormflow in these cases arises mainly from direct rainfall interception by the channel rather than delayed soil water release.

While the depth and distribution of soil layers likely influence the watershed's overall water

storage capacity, observed SWC data showed minimal spatial variability across locations within the watershed. This suggests that SWC can serve as a reasonable proxy for~~reliably represent~~ the watershed's overall soil water storage capacity.

One limitation of this study lies in the indirect estimation of field capacity ~~through~~ using observed SWC thresholds instead of~~rather than~~ direct measurement or modeling. Although this approach aligns with observed patterns and simplifies the analysis, it does not fully capture the spatial variability of field capacity or its dependence on soil depth. Future work should incorporate direct field capacity measurements or modeling to refine the relationship between SWC and delayed stormflow initiation, thereby improving the accuracy of threshold predictions.

4.4 Conceptual model of runoff generation in XEW

This section presents a conceptual model elucidating the runoff generation mechanisms in XEW, with a particular focus on the interplay between soil water storage and GWL dynamics. Soil water storage is identified as the critical factor driving the transition from initial to delayed runoff generation. Once the soil water deficit is replenished, the gradual~~slowl~~y rising GWL becomes the dominant control in the delayed stormflow process. Fig. 17 illustrates the conceptual framework, which incorporates transmissivity feedback mechanisms to explain the formation of distinct hydrograph patterns.

a) Runoff generation under dry conditions (Fig. 17b):

In dry watershed conditions, characterized by low antecedent moisture and light rainfall, rainwater primarily infiltrates and is retained in the soil profiles. Streamflow during such events consists of two primary components: (1) a rapid yet modest streamflow peak driven by direct rainfall onto the channel and (2) a relatively stable baseflow originating from the gradual release of deep groundwater reservoirs.

Under these conditions, ~~the~~ baseflow is primarily sustained by the gradual release of groundwater from~~reflects the slow release of groundwater stored in~~ deeper aquifers. The~~, while the~~

limited rainfall input fails to establish substantial~~is insufficient to trigger significant~~ connectivity between hillslopes and the channel.

b) Delayed stormflow during moderate storms (Fig. 17c):

As rainfall intensity and duration increase, moderate storm events lead to the replenishment of soil water deficits, resulting in the exceedance of soil storage capacity. Initially, the runoff response mirrors that observed under~~resembles that of~~ dry conditions, with a rapid streamflow peak generated by direct channel rainfall. However, as rainfall continues, excess water infiltrates deeper, elevating the GWL and expanding the saturated zone.

This process enhances the hydraulic connectivity between the stream channel and adjacent hillslopes, facilitating the lateral transport of shallow groundwater to the channel. As the GWL rises into~~intersects~~ more conductive soil layers, a delayed stormflow peak emerges~~is observed~~, typically occurring after rainfall ceases. This secondary peak reflects the combined effects of deep infiltration, gradual GWL rise, and increased transmissivity in the subsurface, which accelerates shallow groundwater movement towards the channel.

c) Runoff generation during extreme storm events (Fig. 17d):

Extreme storm events, characterized by high rainfall intensity and large volumes, result in a sharp and widespread rise in GWL across the entire watershed. During such events, the rapid expansion of saturated areas and the increased hydraulic conductivity of the subsurface enable the swift mobilization of shallow groundwater. This synchronous response generates a pronounced flood peak within a short timeframe.

In the riparian zones, GWLs may rise into the soil profile or even reach the ground surface, facilitating direct water flow into the channel via subsurface pathways. Observational data from extreme events corroborate this mechanism, as significant increases in SWC are recorded in the deeper soil layers of riparian zones after rainfall ends. This pattern suggests that groundwater from adjacent hillslopes contributes to the replenishment of soil water in these zones, thereby enhancing

587 the~~reinforcing~~ lateral transport of subsurface flow towards the channel~~pathways~~.

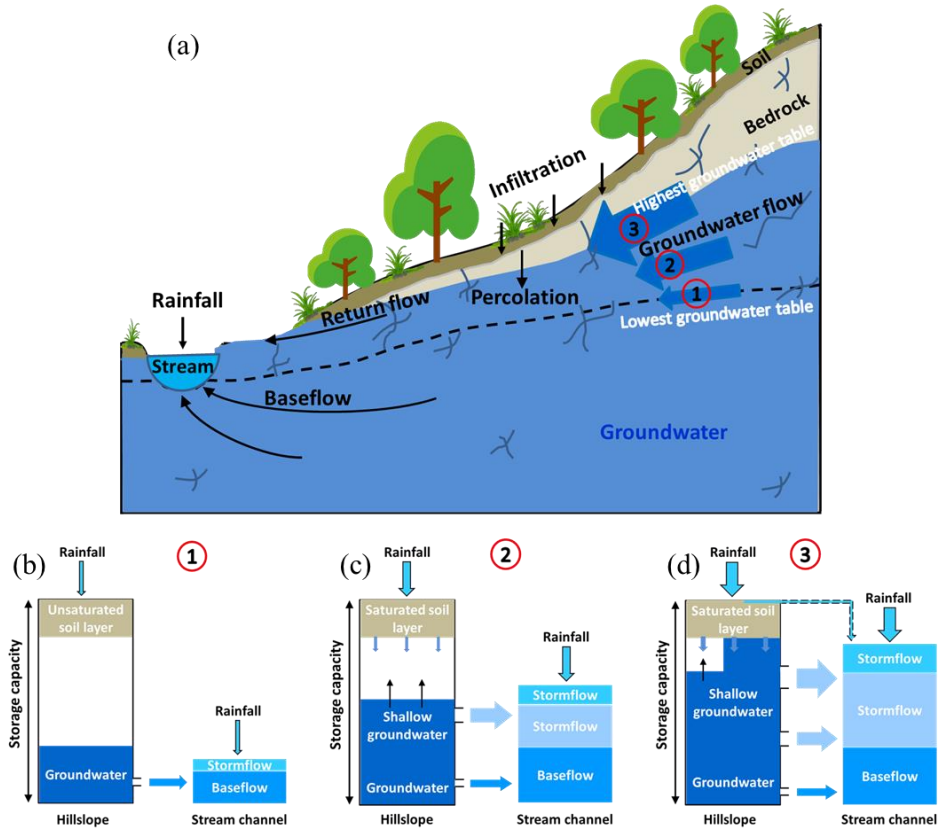

588

589 **Figure 17.** Conceptual model illustrating stormflow generation associated with the transmissivity
590 feedback.

591 The progression from the runoff generation under dry conditions (Fig. 17b) to moderate storm
592 scenarios (Fig. 17c) and ultimately extreme events (Fig. 17d) reflects the progressive wetting-up of
593 the watershed. Abrupt changes in stormflow volume and timing are initially governed by soil water
594 storage thresholds and subsequently controlled by the bedrock hydraulic conductivity ~~of the bedrock~~
595 ~~and micro-topography~~.

This conceptual model provides a theoretical~~quantitative~~ framework for understanding how variations in hydrological conditions influence runoff generation processes in XEW. By integrating soil water storage dynamics, GWL responses, and transmissivity feedback mechanisms, the model offers insights into the nonlinear behavior of runoff processes under different rainfall scenarios.

5. Conclusions

Building upon previous work that identified and characterized bimodal streamflow patterns in XEW, this study quantitatively analyzed SWC and GWL dynamics at the event scale to elucidate the mechanisms driving delayed stormflow generation. The findings reveal that when soil water storage surpasses its holding capacity, a secondary increase in streamflow is triggered. This secondary, or delayed, stormflow is primarily governed by GWL dynamics, which dictate both the magnitude and timing of the delayed response~~ and the lag time to its peak~~.

During rainfall events, SWC responds rapidly, increasing until the soil's water storage capacity is reached or exceeded. If the stored water remains below~~within~~ this capacity, SWC stabilizes or decreases gradually after~~following the cessation of~~ rainfall ceases, eventually leveling off near the field capacity. The rate of this decrease is closely linked to the extent of SWC exceeding the field capacity. When SWC begins to decline, excess rainwater percolates deeper into the soil, raising the GWL. Once GWL begins to rise, it becomes the dominant driver of the delayed stormflow process.

As GWL rises, increased transmissivity facilitates~~hydraulic conductivity increases, facilitating~~ enhanced groundwater flux from hillslopes to the stream channel. This process expands the effective connectivity between the channel and adjacent hillslopes. When~~At specific high~~ GWL exceeds certain thresholds, synchronized ~~the synchronization of GWL~~ responses across multiple hillslopes significantly ~~amplifies~~ amplify stormflow volume. This synchronized behavior~~response~~ shortens the~~shortens the~~ lag time and increases the~~ volume of~~ delayed stormflow volume, often causing~~merging~~ the delayed peak to merge with the direct stormflow peak.

These findings offer critical insights into the nonlinear processes governing stormflow

generation and the formation of bimodal hydrographs. By elucidating the mechanisms underpinning these dynamics, the study advances hydrological theory and provides actionable knowledge for improving flood modeling and prediction.

Data availability

The data supporting this study are available on the Zenodo website at https://doi.org/10.5281/zenodo.12581739.

Author contribution

ZC contributed the conceptualization, formal analysis, investigation and writing; FT contributed the conceptualization, formal analysis and revision.

Competing interests

Fuqiang Tian is a member of the editorial board of Hydrology and Earth System Sciences.

Acknowledgements

This study was supported by National Key R&D Program of China (2022YFC3002902) and National Natural Science Foundation of China (51825902).

5. References

Anderson, M. G., and Burt, T. R.: The role of topography in controlling throughflow generation, Earth Surf. Process., 3, 331–334, https://doi.org/10.1002/esp.3290030402, 1978.

Beiter, D., Weiler, M., and Blume, T.: Characterising hillslope–stream connectivity with a joint event analysis of stream and groundwater levels, Hydrol. Earth Syst. Sci., 24, 5713-5744, https://doi.org/10.5194/hess-24-5713-2020, 2020.

Bishop, K., Seibert, J., Nyberg, L., and Rodhe, A.: Water storage in a till catchment. II: Implications of transmissivity feedback for flow paths and turnover times, Hydrol. Process., 25, 3950-3959, https://doi.org/10.1002/hyp.8355, 2011.

Cui, Z., Tian, F., Zhao, Z., Xu, Z., Duan, Y., Wen, J., and Khan, M. Y. A.: Bimodal Hydrographs in Semi-humid

Forested Watershed: Characteristics and Occurrence Conditions, Hydrol. Earth Syst. Sci. Discuss., https://doi.org/10.5194/hess-2024-36, 2024.

Dang, L., Xie, Y. Q., Wang, C., Chang, Y., Zeng, X. K., and Wu, J. C.: Precipitation-induced Pressure Wave Propagation in Unsaturated Zone and Its Effect on Rapid Groundwater Discharge, Geol. J. China Univ., 29, 580-589, https://doi.org/10.16108/j.issn1006-7493.2021104, 2023.

Detty, J. M., and McGuire, K. J.: Threshold changes in storm runoff generation at a till-mantled headwater catchment, Water Resour. Res., 46, W07525, https://doi.org/10.1029/2009WR008102, 2010.

Farrick, K. K., and Branfireun, B. A.: Soil water storage, rainfall and runoff relationships in a tropical dry forest catchment, Water Resour. Res., 50, 9236-9250, https://doi.org/10.1002/2014WR016045, 2014.

Graeff, T., Zehe, E., Reusser, D., Lück, E., Schröder, B., Wenk, G., John, H., and Bronstert, A.: Process identification through rejection of model structures in a mid-mountainous rural catchment: observations of rainfall-runoff response, geophysical conditions and model inter-comparison, Hydrol. Process., 23, 702–718, https://doi.org/10.1002/hyp.7171, 2009.

Graham, C. B., and McDonnell, J. J.: Hillslope threshold response to rainfall: (2) development and use of a macroscale model, J. Hydrol., 393, 77–93, https://doi.org/10.1016/j.jhydrol.2010.03.008, 2010.

Graham, C. B., Woods, R. A., and McDonnell, J. J.: Hillslope threshold response to rainfall: (1) A field based forensic approach, J. Hydrol., 393, 65–76, https://doi.org/10.1016/j.jhydrol.2009.12.015, 2010.

Haga, H., Matsumoto, Y., Matsutani, J., Fujita, M., Nishida, K., and Sakamoto, Y.: Flow paths, rainfall properties, and antecedent soil moisture controlling lags to peak discharge in a granitic unchanneled catchment, Water Resour. Res., 41, W2179–W2187, https://doi.org/10.1029/2005wr004236, 2005.

Haught, D. R. W. and Meerveld, H. J.: Spatial variation in transient water table responses: differences between an upper and lower hillslope zone, Hydrol. Process., 25, 3866-3877, https://doi.org/10.1002/hyp.8354, 2011.

Hewlett, J. D., and Hibbert, A. R.: Factors affecting the response of small watersheds to precipitation in humid areas, in: Forest Hydrology, edited by: Sopper, W. E. and Lull, H. W., Pergamon Press, Oxford, 275–290, 1967.

Kendall, K. A., Shanley, J. B., and McDonnell, J. J.: A hydrometric and geochemical approach to test the transmissivity feedback hypothesis during snowmelt, J. Hydrol., 219, 188–205, https://doi.org/10.1016/S0022-1694(99)00059-1, 1999.

Kosugi, K., Fujimoto, M., Katsura, S., Kato, H., Sando, Y., and Mizuyama, T.: Localized bedrock aquifer distribution explains discharge from a headwater catchment, Water Resour. Res., 47, W07111, https://doi.org/10.1029/2010WR009884, 2011.

Lundin, L.: Soil moisture and ground water in till soil and the significance of soil type for runoff, PhD Thesis, Uppsala University, UNGI Report No. 56, 216 pp., 1982.

Martínez-Carreras, N., Hissler, C., Gourdol, L., Klaus, J., Juilleret, J., Iffly, J. F., and Pfister, L.: Storage controls on the generation of double peak hydrographs in a forested headwater catchment, J. Hydrol., 543, 255–269, https://doi.org/10.1016/j.jhydrol.2016.10.004, 2016.

McDonnell, J. J., Spence, C., Karran, D. J., Van Meerveld, H. J., and Harman, C. J.: Fill-and-spill: A process

681 description of runoff generation at the scale of the beholder, Water Resour. Res., 57, e2020WR027514,
682 https://doi.org/10.1029/2020WR027514, 2021.
683 Padilla, C., Onda, Y., and Iida, T.: Interaction between runoff–bedrock groundwater in a steep headwater catchment
684 underlain by sedimentary bedrock fractured by gravitational deformation, Hydrol. Process., 29, 4398–4412,
685 https://doi.org/10.1002/hyp.10498, 2015.
686 Penna, D., Tromp-van Meerveld, H. J., Gobbi, A., Borga, M., and Dalla Fontana, G.: The influence of soil moisture
687 on threshold runoff generation processes in an alpine headwater catchment, Hydrol. Earth Syst. Sci., 15, 689-
688 702, https://doi.org/10.5194/hess-15-689-2011, 2011.
689 Rinderer, M., van Meerveld, I., Stähli, M., and Seibert, J.: Is groundwater response timing in a pre-alpine catchment
690 controlled more by topography or by rainfall? Hydrol. Process., 30, 1036-1051,
691 https://doi.org/10.1002/hyp.10634, 2016.
692 Scaife, C. I., Singh, N. K., Emanuel, R. E., Miniat, C. F., and Band, L. E.: Non-linear quickflow response as
693 indicators of runoff generation mechanisms, Hydrol. Process., 34, 2949–2964,
694 https://doi.org/10.1002/hyp.13780, 2020.
695 Sloto, R. A., and Crouse, M. Y.: HYSEP: A computer program for streamflow hydrograph separation and analysis,
696 US Geol. Surv., https://doi.org/10.3133/wri964040, 1996.
697 Tian, F., Li, H., and Sivapalan, M.: Model diagnostic analysis of seasonal switching of runoff generation
698 mechanisms in the blue river basin, Oklahoma, J. Hydrol., 418-419, 136–149,
699 https://doi.org/10.1016/j.jhydrol.2010.03.011, 2012.
700 Tromp-van Meerveld, H. J., and McDonnell, J. J.: Threshold relations in subsurface stormflow: 1. A 147-storm
701 analysis of the Panola hillslope, Water Resour. Res., 42, W02410, https://doi.org/10.1029/2004WR003778,
702 2006a.
703 Tromp-van Meerveld, H. J., and McDonnell, J. J.: Threshold relations in subsurface stormflow: 2. The fill and spill
704 hypothesis, Water Resour. Res., 42, W02411, https://doi.org/10.1029/2004WR003800, 2006b.

705

Appendix A:

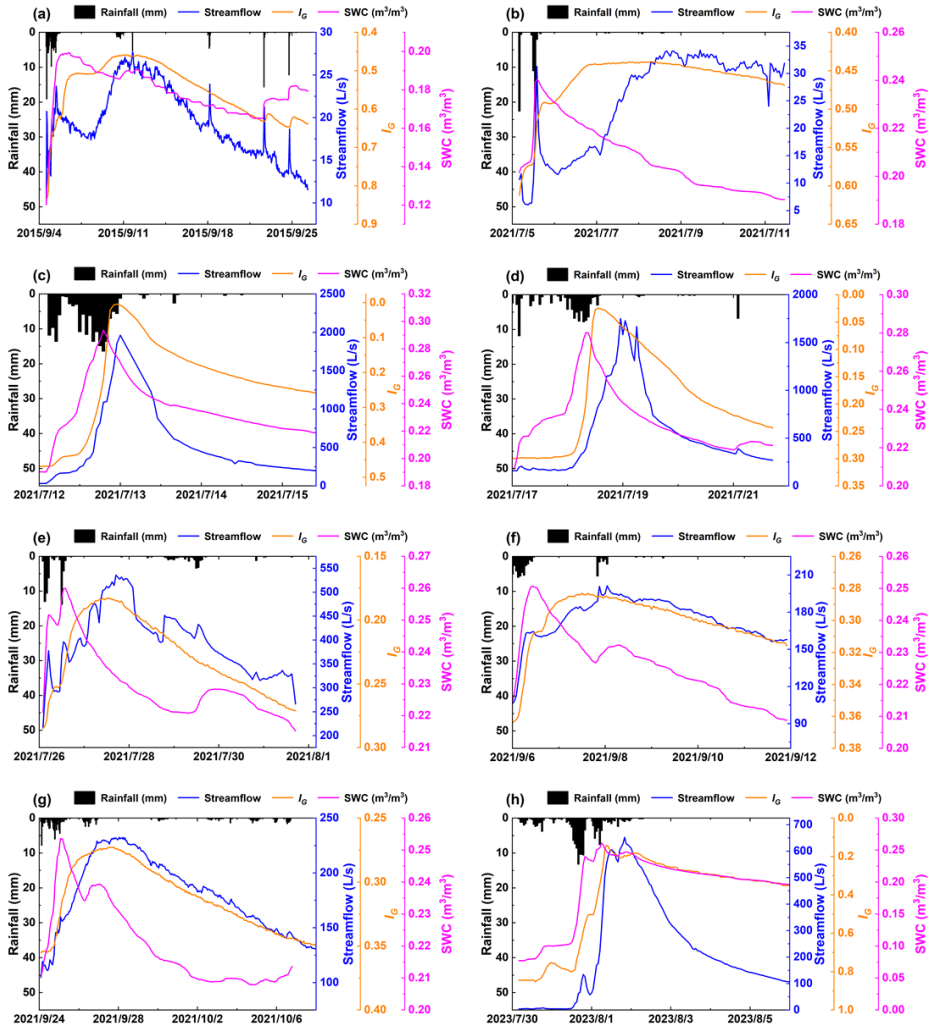

Figure A1. Examples of responses of streamflow, I_G and soil water content to rainfall.